Progress In Electromagnetics Research, PIER 45, 1–20, 2004

COIFMAN WAVELETS IN ELECTROMAGNETIC WAVE SCATTERING BY A GROOVE IN A CONDUCTING PLANE

Y. Tretiakov

IBM Microelectronics
Essex Junction, VT 05452, USA

G. Pan

Department of Electrical Engineering
Arizona State University
Tempe, AZ 85287, USA

Abstract—Scattering of electromagnetic waves from a groove in an infinite conducting plane is studied using the Coifman wavelets (Coiflets) under the integral equation formulation. The induced current is expressed in terms of the known Kirchhoff solution plus a localized correction current in the vicinity of the groove. The Galerkin procedure is implemented, employing the Coiflets as expansion and testing functions to find the correction current numerically. Owing to the vanishing moments, the Coiflets lead to a one-point quadrature formula in $O(h^5)$, which reduces the computational effort in filling the impedance matrix entries. The resulting matrix is sparse, which is desirable for iterative algorithms. Numerical results show that the new method is 2 to 5 times faster than the pulse based method of moments.

1 Introduction

2 Hybrid PO-MoM Formulation

3 Basic Principles of Orthogonal Wavelets

4 Coifman Based MoM

5 BI-CGSTAB Algorithm

6 Numerical Results

7 Conclusions

References

1. INTRODUCTION

Scattering of electromagnetic waves from a 2D groove in an infinite conducting plane has been studied in [1] using the hybrid PO-MoM technique, where Haar wavelets were implemented to solve the integral equation. While their formulation is excellent, the computational efficiency of their approach may be less effective than the standard MoM [2], due to the poor performance of the Haar wavelets. In recent years, wavelets have found application in computational electromagnetics. Usually, wavelets are defined on the whole real line, while many practical problems are restricted to finite intervals. Therefore, wavelets have to be modified so they can be easily adopted on the finite interval to solve boundary value problems. Examples of such modified wavelets are intervallic [3] and periodic [4] wavelets. At the same time, the simple Haar wavelets seem to be able to handle the boundaries easily, but the move from advanced wavelets to the oldest Haar wavelets is a leap backward.

In this paper we modified the formulation in [1] to employ the Coifman wavelets (Coiflets) in combination with the physical optics approach [5]. The Coiflets possess one-point quadrature and thus are used for the hybrid PO-MoM technique. This reduces the computational effort in filling the MoM impedance matrix entries. As a result, the Coifman wavelet approach with two-fold integration is faster than that of the traditional pulse based one-fold integration. The difficulty of using wavelets in dealing with boundaries is bypassed by [1] formulation, because the local correction current smoothly decays to negligible level without a sharp boundary. As a result, the Coifman wavelets are used on a finite interval without any modification (such as the periodic wavelets or intervallic wavelets). Following [1], the unknown induced current is expressed in terms of the known PO current of the scattering by an infinite conducting plane plus the localized correction current placed in the vicinity of the groove. Due to its local nature, the correction current spreads out only several wavelengths from the groove.

The localized correction current is numerically evaluated using the Coiflets under Galerkin's procedure [6, 7]. The obtained system of linear equations is solved using the standard LU decomposition [8] and the iterative BI-CGSTAB [9] technique. When the size of the impedance matrix is large, the BI-CGSTAB method is faster than the LU decomposition approach, especially when sparse matrices are involved.

2. HYBRID PO-MOM FORMULATION

The PO-MoM formulation was derived in [1]. For ease of references, we quoted the major steps of the formulation in [1] here, upon which our modification was built. We also added the TE_z case here, in addition to TM_z time-harmonic electromagnetic plane waves in the aforementioned reference.

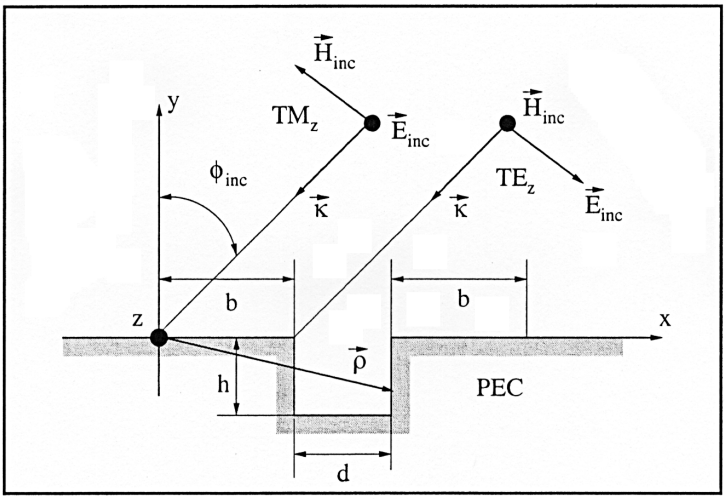

Figure 1. Geometry of the two-dimensional groove in a conducting plane.

The cross-sectional view of the two-dimensional scattering problem is shown in Figure 1. The angle of incidence ϕ_{inc} is measured with respect to the y axis. The depth and width of the groove are h and d, respectively. For the TM_z polarization of the incident plane wave the induced current $\vec{J}_s$ is z-directed and independent of z, that is $\vec{J}_s = \hat{z} \cdot J_z(x, y)$. For the TE_z scattering case current $\vec{J}_s$ is also z-independent and lies in the (x, y) plane.

First, we consider the case of the TM_z scattering. We split the geometry of our scattering problem into segments $\{l_s\}$, $s = 1, \ldots, 6$, as shown in Figure 2.

The segments l_1 and l_5 are semi-infinite. We write J_z in terms of four current distributions J^{PO}, J_L^{PO}, J_C and $\tilde{J}_C$ as

$$J_z = J^{PO} - J_L^{PO} + J_C + \tilde{J}_C. \tag{1}$$

In the Equation (1) we partitioned the induced current J_z into the

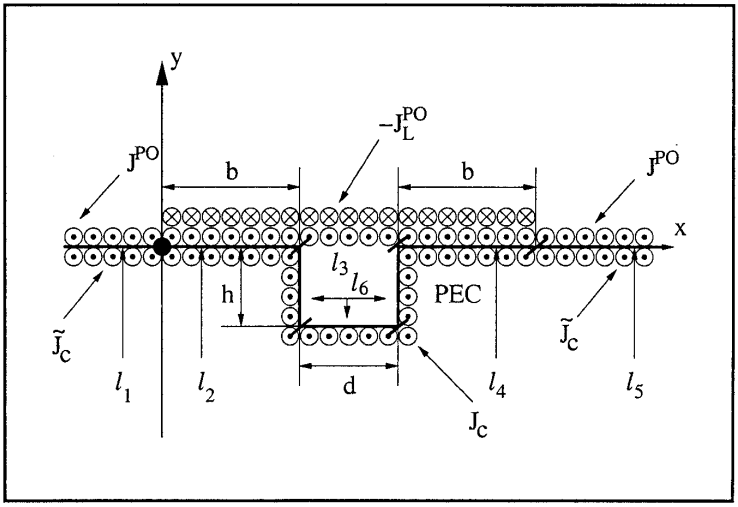

Figure 2. The partition of the induced current J_z.

following components:

i. J^{PO} is the known physical optics current solution of the unperturbed problem (the current that would be induced on a perfectly infinite plane formed by $\cup_{s=1}^{5} l_s$).

ii. J_L^{PO} is the portion of the physical optics current J^{PO} residing on $\cup_{s=2}^{4} l_s$.

iii. J_C is the unknown surface *correction* current on the groove region l_6 and its vicinity l_2 and l_4.

iv. $\tilde{J}_C$ is the unknown surface correction current, defined on l_1 and l_5.

The widths of the segments l_2 and l_4 are chosen sufficiently large to ensure that on the segments l_1 and l_5 the induced current is essentially equal to the physical optics current J^{PO} on an infinite plane.

The following boundary condition is used on the surface of the perfect conductor

$$L_z^s(J_z) + E_z^{inc} = 0 \quad \text{on} \quad l_t. \tag{2}$$

to find the induced current J_z, where the operator $L_z^s(\cdot)$ denotes the scattered electric field component which is tangential to the surface of the groove scatterer and due to the current J_z and $l_t = l_1 \cup l_2 \cup l_6 \cup$

$l_4 \cup l_5$. The electric field component E_z^{inc} is the tangential component of the incident electric field. From (1) and (2) one obtains

$$L_z^s\left(J^{PO} - J_L^{PO} + J_C + \tilde{J}_C\right) + E_z^{inc} = 0 \quad \text{on} \quad l_t. \tag{3}$$

The operator $L_z^s(\cdot)$, which describes the scattered field is a linear function of the induced current and thus

$$L_z^s(J^{PO}) - L_z^s(J_L^{PO}) + L_z^s(J_C) + L_z^s(\tilde{J}_C) = -E_z^{inc} \quad \text{on} \quad l_t. \tag{4}$$

We should notice here that the electric field due to the physical optics current J^{PO} will cancel the incident field E_z^{inc} on and below of the surface $\cup_{s=1}^5 l_s$. It means that

$$L_z^s(J^{PO}) = -E_z^{inc} \quad \text{on} \quad l_t. \tag{5}$$

If we combine (4) and (5) together, then we obtain

$$L_z^s(J_C + \tilde{J}_C) = L_z^s(J_L^{PO}) \quad \text{on} \quad l_t. \tag{6}$$

We can further simplify the Equation (6) if we recall that the induced current on l_1 and l_5 is almost equal to the physical optics current J^{PO}. This gives the following approximation

$$\tilde{J}_C \approx 0. \tag{7}$$

From (7) and (6) it immediately follows that $L_z^s(\tilde{J}_c) \approx 0$ and hence

$$L_z^s(J_C) = L_z^s(J_L^{PO}) \quad \text{on} \quad l_t, \tag{8}$$

where the right-hand side is the known tangential electric field due to the current J_L^{PO}, while J_C is the unknown correction current. The correction current J_C is defined on $l_2 \cup l_6 \cup l_4$ and therefore (8) can be rewritten in the following way

$$L_z^s(J_C) = L_z^s(J_L^{PO}) \quad \text{on} \quad l_2 \cup l_6 \cup l_4. \tag{9}$$

For the TM_z scattering the operator $L_z^s(\cdot)$ has the following form

$$L_z^s(J) = -\frac{\kappa\eta}{4}\int_l J(\vec{\rho}\,')H_0^{(2)}(\kappa|\vec{\rho} - \vec{\rho}\,'|)dl', \tag{10}$$

where κ is the wave number, $\eta = \sqrt{\mu_0/\epsilon_0}$, $H_0^{(2)}$ is the Hankel function of the second kind of order 0 and $e^{j\omega t}$ time convention is used. Therefore, we can rewrite (9) as follows

$$\int_{l_2+l_6+l_4} J_C(\vec{\rho}\,')H_0^{(2)}(\kappa|\vec{\rho} - \vec{\rho}\,'|)dl' = \int_{l_2+l_3+l_4} J_C^{PO}(\vec{\rho}\,')H_0^{(2)}(\kappa|\vec{\rho} - \vec{\rho}\,'|)dl', \tag{11}$$

where $\vec{\rho} \in l_2 \cup l_6 \cup l_4$.

Eq. (11) is sufficient for the determination of the correction current J_C The unknown current J^C is defined on the finite segments $l_2 \cup l_6 \cup l_4$ and is almost equal to the physical optics current J^{PO} at the starting and end points of the interval. The integral equation (11) is solved numerically using the MoM. To use the Coifman wavelets without any modification in the MoM on the finite interval, we change (11) to another form. The idea is to modify the integral equation (11) into a form for which the solution is essentially zero at the end points of the computational interval and beyond. For our correction current J^C we know that it is approximately equal to the physical optics current J^{PO} at the end points of the interval l_2 and l_4. We then subtract the known current J^{PO} defined on the intervals l_2 and l_4 from the unknown current J^C by doing so, we tailor (11) into the following form

$$\int_{l_2+l_6+l_4} J_C(\vec{\rho}\,')H_0^{(2)}(\kappa|\vec{\rho}-\vec{\rho}\,'|)dl' - \int_{l_2+l_4} J_L^{PO}(\vec{\rho}\,')H_0^{(2)}(\kappa|\vec{\rho}-\vec{\rho}\,'|)dl' = \int_{l_3} J_L^{PO}(\vec{\rho}\,')H_0^{(2)}(\kappa|\vec{\rho}-\vec{\rho}\,'|)dl'. \quad (12)$$

Let us define a new unknown current

$$J_p = \begin{cases} J_C & \text{on} \quad l_6, \\ J_C - J_L^{PO} & \text{on} \quad l_2 \cup l_4. \end{cases} \quad (13)$$

Using the above unknown current J_p, we rewrite (12) in a compact form

$$\int_{l_2+l_6+l_4} J_p(\vec{\rho}\,')H_0^{(2)}(\kappa|\vec{\rho}-\vec{\rho}\,'|)dl' = \int_{l_3} J_L^{PO}(\vec{\rho}\,')H_0^{(2)}(\kappa|\vec{\rho}-\vec{\rho}\,'|)dl', \quad \vec{\rho} \in l_2 \cup l_6 \cup l_4. \quad (14)$$

Eq. (14) is the finite form of the new PO-MoM integral equation formulation. To solve the unknown current J_p in (14), we first expand J_p in terms of the basis functions $\{q_i\}_{i=1}^N$ defined on $l_2 \cup l_6 \cup l_4$ as

$$J_p = \sum_{n=1}^{N} a_n q_n. \quad (15)$$

We then conduct Galerkin's procedure to discretize the integral equation (14) into a matrix equation

$$[Z][I] = [V] \quad (16)$$

where

$$Z_{mn} = \int_{s_m}\int_{s_n} q_m(l)q_n(l')H_0^{(2)}(\kappa|\vec{\rho}-\vec{\rho}'|)dl'dl, \tag{17}$$

$$I_n = a_n, \tag{18}$$

$$V_m = \int_{s_m}\int_{l_3} q_m(l)J_L^{PO}(l')H_0^{(2)}(\kappa|\vec{\rho}-\vec{\rho}'|)dl'dl. \tag{19}$$

In the previous equations s_m denotes the support of the basis function q_m. By solving (16) numerically one may obtain an approximate solution for the scattering problem of Fig. 1 with a finite number of unknowns.

To evaluate V_m of the right-hand side in (14), we use (19), in which the physical optics current J_L^{PO} for the TM_z scattering is given in [5] as

$$\vec{J}_L^{PO} = 2\hat{n}\times\vec{H}_{inc}. \tag{20}$$

More specifically, the incident electric and magnetic fields are

$$\vec{E}_{inc} = \hat{z}\cdot\eta\cdot e^{j\kappa(x\sin\phi_{inc}+y\cos\phi_{inc})} \tag{21}$$

$$\vec{H}_{inc} = (-\hat{x}\cdot\cos\phi_{inc}+\hat{y}\cdot\sin\phi_{inc})e^{j\kappa(x\sin\phi_{inc}+y\phi_{inc})}. \tag{22}$$

where the time convention again is understood and suppressed. Upon substituting (22) into (20) one obtains

$$\vec{J}_L^{PO} = \hat{z}\cdot 2\cos\phi_{inc}\cdot e^{j\kappa x\sin\phi_{inc}}. \tag{23}$$

The TE_z scattering can be formulated in a similar way. For the sake of simplicity we omit the detailed derivation of the TE_z case and only present the final equation to be solved

$$\begin{aligned} &J_p(\vec{\rho})\left(-\frac{j}{\pi}\right)+\int_{l_2+l_6+l_4} J_p(\vec{\rho}')H_1^{(2)}(\kappa|\vec{\rho}-\vec{\rho}'|)\cos\psi' dl' \\ &= \int_{l_3} J_L^{PO}(\vec{\rho}')H_1^{(2)}(\kappa|\vec{\rho}-\vec{\rho}'|)\cos\psi' dl', \quad \vec{\rho}\in l_2\cup l_6\cup l_4, \end{aligned} \tag{24}$$

with

$$\vec{J}_L^{PO} = \hat{x}\cdot 2\cdot e^{j\kappa x\sin\phi_{inc}}, \tag{25}$$

where

$$\cos\psi' = \frac{\vec{n}'\cdot(\vec{\rho}-\vec{\rho}')}{|\vec{\rho}-\vec{\rho}'|}, \tag{26}$$

$\vec{n}'$ is the unit normal placed at the source point on the groove surface and $H_1^{(2)}$ is the Hankel function of the second kind of order 1.

3. BASIC PRINCIPLES OF ORTHOGONAL WAVELETS

Basic wavelet theory can be found in many excellent books [7, 10, 11]. However, for readers without rigorous mathematical training, it is not a trivial task to comprehend some of the main concepts and convert them into meaningful engineering tools. In this section we briefly list basic wavelet principles that are used to construct and facilitate the wavelets. A multiresolution analysis of $L^2(R)$ is defined as a sequence of closed subspaces V_j of $L^2(R)$, $j \in Z$. A scaling function $\varphi(x) \in V_0$, with a non-vanishing integral, exists such that the collection $\{\varphi(t-l)|l \in Z\}$ forms a Riesz basis of V_0.

Since $\varphi \in V_0 \subset V_1$, a sequence $\{h_k\} \in \ell^2$ exists such that the scaling function satisfies

$$\varphi(x) = \sqrt{2}\sum_k h_k \varphi(2x-k). \tag{27}$$

This functional equation is referred to as the dilation equation, where $\{h_k\}$ are coefficients of the lowpass filter, and

$$\sum_k h_k = 1. \tag{28}$$

The collection of functions $\{\varphi_{j,l}|l \in Z\}$, with

$$\varphi_{j,l}(x) = 2^{j/2}\varphi(2^j x - l) \tag{29}$$

forms a Riesz basis of V_j.

We will use W_j to denote a space complementing V_j in V_{j+1}, that is, a space that satisfies

$$V_{j+1} = V_j \otimes W_j \tag{30}$$

and

$$\bigotimes_j W_j = L^2(R). \tag{31}$$

A function ψ is a wavelet if the collection of functions $\{\psi(x-l)|l \in Z\}$ forms a Riesz basis of W_0. The collection of wavelet functions $\{\psi_{j,l}|l, j \in Z\}$ then forms a Riesz basis of $L^2(R)$. The definition of $\psi_{j,l}$ is similar to that of $\varphi_{j,l}$. Since the wavelet ψ is an element of V_1, a sequence $\{g_k\} \in \ell^2(R)$ exists such that

$$\psi(x) = \sqrt{2}\sum_k g_k \varphi(2x-k). \tag{32}$$

In the previous equation, the bandpass filter for the orthogonal wavelets can be represented by the lowpass filters as

$$g_k = (-1)^{k-1} h_{-(k-1)}. \tag{33}$$

In addition to the general properties of the orthogonal wavelet family, the Coifman scaling functions have a unique feature. Let us select the orthogonal Coifman scaling function with $6N$ non-zero coefficients, where $L = 2N$ is the order of the Coifman wavelets. The Coifman wavelets have the vanishing moments properties in both scaling functions and wavelets, namely

$$\int \varphi(x)dx = 1, \tag{34}$$

$$\int x^p \varphi(x)dx = 0, \qquad p = 1, 2, \ldots, 2N-1, \tag{35}$$

$$\int x^p \psi(x)dx = 0, \qquad p = 0, 1, 2, \ldots, 2N-1. \tag{36}$$

Scaling functions under the L^2 norm exhibit Dirac-δ like sampling property for smooth functions. Namely, if $\varphi(x)$ is supported in $[p, q]$, and we expand $f(x)$ at a point x_0 within $[p, q]$, then

$$\begin{aligned} & \int_p^q f(x)\varphi(x - x_0)dx \\ = & \int_p^q \left(f(x_0) + f'(x_0)(x - x_0) + \cdots + \frac{f^{2N-1}(x_0)(x - x_0)^{2N-1}}{(2N-1)!} + \cdots \right) \\ & \cdot \varphi(x - x_0)dx \\ = & f(x_0) + O(h^{2N}) \end{aligned} \tag{37}$$

where h is the discretization size. This property in a simple sense is similar to Dirac-δ function property

$$\int f(x)\delta(x - x_0)dx = f(x_0). \tag{38}$$

Of course, the Dirac-δ function is the extreme example of localization in the space domain, with infinite number of vanishing moments. The Dirac-δ like nature of the Coiflets allows us to simplify a numerical integration into a single point value, and thus speeds up the matrix element evaluations greatly.

4. COIFMAN BASED MOM

The Coifman scaling functions of order $L = 2N$ and resolution level j_0 were employed as the basis functions to expand the unknown surface current J_p in (14) in the form

$$J_p(t') = \sum_n a_n \varphi_{j_0,n}(t'), \tag{39}$$

where $\varphi_{j_0,n}(t') = 2^{j_0/2}\varphi(2^{j_0}t' - n)$. Again, all equations are presented only for the TM_z scattering and TE_z case is treated in the same way.

After testing the integral equation (14) with the same Coifman scaling functions $\{\varphi_{j_0,m}(t)\}$, we have the impedance matrix with the mn-th entry

$$Z_{m,n} = \int_{S_m}\int_{S_n} H_0^{(2)}(\kappa|\vec{\rho}(t) - \vec{\rho}'(t')|)\varphi_{j_0,m}(t)\varphi_{j_0,n}(t')dt'dt \tag{40}$$

and

$$V_m = \int_{S_m}\int_{l_3} \varphi_{j_0,m}(t) J_L^{PO}(t') H_0^{(2)}(\kappa|\vec{\rho}(t) - \vec{\rho}'(t')|)dt'dt \tag{41}$$

where S_n and S_m are supports of the expansion and testing wavelets, respectively.

The following one point integration rule [3]

$$\int_{S_m}\int_{S_n} H_0^{(2)}(t,t')\varphi_{j_0,m}(t)\varphi_{j_0,n}(t')dt'dt \approx \frac{1}{2^{j_0}} H_0^{(2)}\left(\frac{m}{2^{j_0}}, \frac{n}{2^{j_0}}\right) \tag{42}$$

is employed to evaluate the system matrix elements for which $H_0^{(2)}(\kappa|\vec{\rho} - \vec{\rho}'|)$ is free of singularity within the interval of integration. To be more specific, the one-point quadrature formula (42) is used to calculate elements of the MoM matrix, for which $|m - n| \geq 1$. In addition to that, it is also used to construct right hand side vector (41).

For all diagonal elements, the kernel of the integral (40) has a singularity at $t = t'$. As a result, the diagonal elements are computed by standard Gauss-Legendre quadrature [8]. We used different number of Gaussian points with respect to t and t' to avoid the case of $t = t'$. For instance, for the standard pulse based MoM, we use 4 and 6 Gaussian points with respect to t' and t. These numbers have been found numerically and they are the minimum numbers of Gaussian points required to get accurate and stable numerical results. At the same time, for the Coifman based MoM we split a support of each

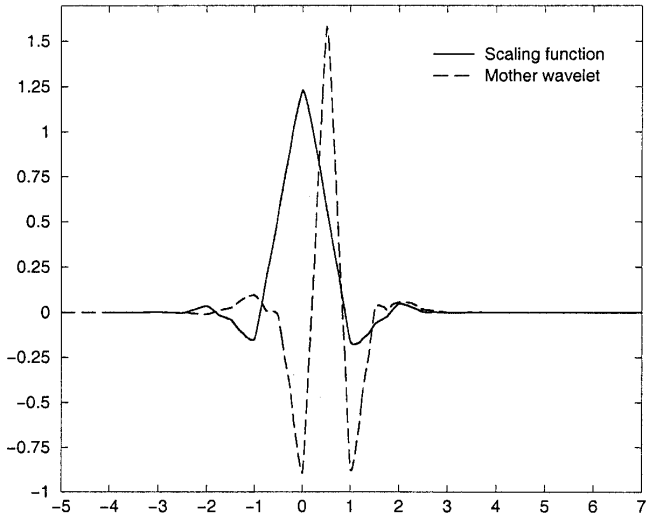

Figure 3. Coifman scaling function and mother wavelet ($L = 4,\ j_0 = 0,\ n = 0$).

scaling function into 5 small segments and used 4 and 6 points on each subinterval to make an integration over t' and t, respectively.

In all numerical examples we applied the Coifman wavelets of order $L = 2N = 4$. Shown in Figure 3 are the Coifman wavelets of order $L = 4$, resolution level $j_0 = 0$, and shift $n = 0$. Although, the higher order Coifman wavelets provide more vanishing moments and produce a better approximation, the support of these wavelets is wider and it would take a longer time to compute the singular integrals in (40). The choice of $L = 4$ is a good trade off between accuracy and computation time.

It has been also noticed that in actual numerical computations the accuracy of the expression (42) depends on a resolution level j_0. The higher the resolution level is, the better result one can get using the one point quadrature rule (42). In this paper, we select the Coifman scaling functions with resolution level $j_0 = 5$ to construct the MoM matrix and then perform the fast wavelet transform (FWT) [12] to obtain the standard form sparse matrix for further numerical computation.

5. BI-CGSTAB ALGORITHM

The solution of the linear algebraic system (16) can be obtained from the standard LU decomposition in combination with the back-

substitution, available in many books on numerical analysis. When the size of the impedance matrix $[Z]$ becomes large, it is better to apply the iterative method to speed up the numerical computation. In this paper, we use the standard LU decomposition technique as well as the stabilized variant of the bi-conjugate gradient (BI-CG) iterative solver, named BI-CGSTAB [9].

It is important to note that the Bi-CGSTAB method does not involve any use of the transpose matrix $[Z]^T$. Therefore, the computation time of matrix manipulation is reduced. The actual stopping criterion in solving $[Z]|x\rangle = |b\rangle$ is to force the residue

$$\|r_i\|_{L_2} < EPS \cdot \|b - Zx_0\|_{L_2} \tag{43}$$

with $EPS = 10^{-5}$. It has been found from the experiment that with this value of the parameter EPS we have quick solution, while maintaining good numerical accuracy.

We also employed the sparse version of the Bi-CGSTAB algorithm when wavelets are involved. The special algorithm from [8] has been adopted to store the sparse matrix in the computer memory. To be more specific, the row-indexed sparse storage technique has been implemented. Moreover, the special algorithm has been also used to compute the fast product of a sparse matrix with a given vector at every iteration step in the Bi-CGSTAB.

6. NUMERICAL RESULTS

Example 1. TM_z scattering from the groove.

Referring to Figure 1, the following dimensions are in use: $b = 3.09375\lambda$, $h = 0.5\lambda$, $d = 0.5\lambda$. While we use 256 Coifman scaling functions to expand the unknown current J_p, we employ 246 pulse bases for comparison. The order of the Coiflets was chosen $L = 2N = 4$ with the resolution level $j_0 = 5$. The obtained numerical results for different incident angles are presented in Figures 4 and 5. We plotted the normalized correction current J_C with respect to the length parameter (arclength) given in wavelength λ. The correction current J_C is evaluated by (13) from the integral equation solution of the unknown current J_p.

Notice, that magnitudes of the normalized current J_C at segment l_2 and l_4 ends are really close to current values (which depend from the angle of incidence for the TM_z mode) predicted by (23).

To demonstrate the advantage of the Coifman wavelets and Bi-CGSTAB algorithm, we present in Tables 1 and 2 the results of the computational time. In the tables, N_p and N_c denote the number of

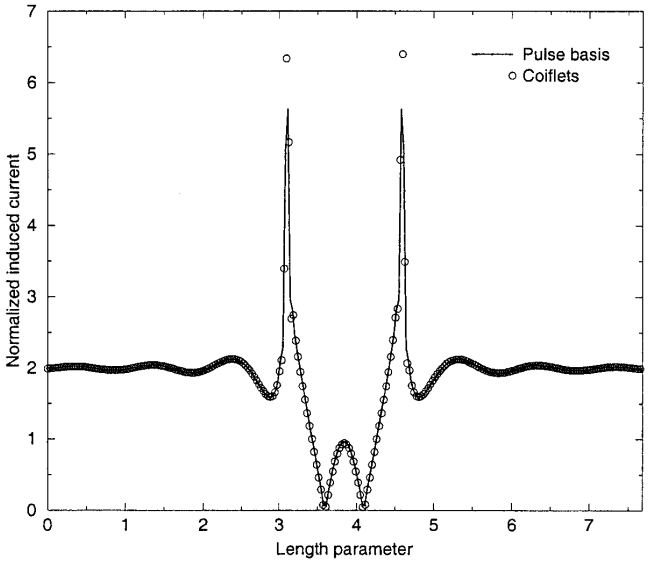

Figure 4. Normalized induced current versus length parameter (λ), TM_z case, $b = 3.09375\lambda$, $h = 0.5\lambda$, $d = 0.5\lambda$, $\phi_{inc} = 0°$, $N_p = 246$, $N_c = 256$.

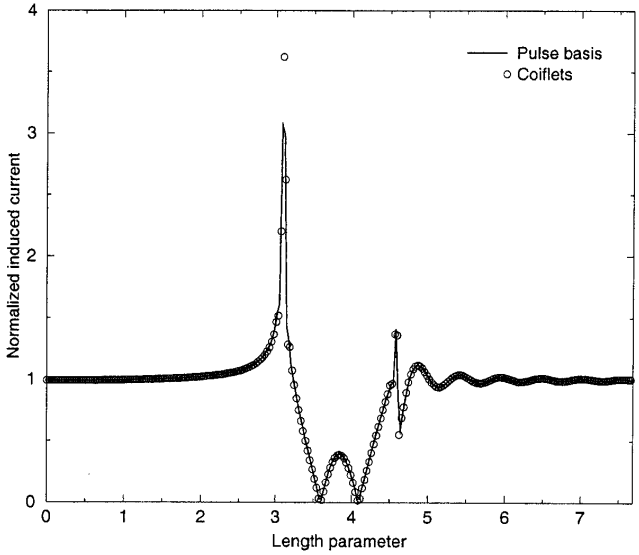

Figure 5. Normalized induced current versus length parameter (λ), TM_z case, $b = 3.09375\lambda$, $h = 0.5\lambda$, $d = 0.5\lambda$, $\phi_{inc} = 60°$, $N_p = 246$, $N_c = 256$.

Table 1. Computation time for the pulse basis, TM_z scattering.

Pulse basis			
N_p	LU time (sec)	Bi-CGSTAB time (sec)	N_{it}
1014	522.86	331.85	61
502	85.94	73.21	44
246	16.57	16.47	33

Table 2. Computation time for the Coifman wavelets, TM_z scattering.

Coifman wavelets						
N_c	LU time (sec)	Bi-CGSTAB time (sec)	N_{it}	Sparse Bi-CGSTAB time (sec)	N_{it}	Sparsity %
1024	354.42	168.82	61	60.91	62	11.94
512	45.94	31.50	43	18.19	45	15.78
256	8.03	8.49	34	6.65	34	22.28

pulses and Coiflets in the MoM, N_{it} is the number of iterations in the Bi-CGSTAB algorithm. The following parameters are used to create data in Tables 1, 2:

- $b=3.09375\lambda,\ h=0.5\lambda,\ d=0.5\lambda,\ \phi_{inc}=60°,\ N_p=246,\ N_c=256$
- $b=6.34375\lambda,\ h=1.0\lambda,\ d=1.0\lambda,\ \phi_{inc}=60°,\ N_p=502,\ N_c=512$
- $b=12.84375\lambda,\ h=2.0\lambda,\ d=2.0\lambda,\ \phi_{inc}=60°,\ N_p=1014,\ N_c=1024$

We implemented LU and Bi-CGSTAB methods to solve a system of linear equations. We also decomposed the system matrix in the Coifman based MoM into a sparse matrix of the standard form using 5 resolution levels. Then, the sparse version of the Bi-CGSTAB is imposed to solve the linear equations. The threshold level of $10^{-4} \cdot p$ has been adjusted to sparsify the system matrix in the MoM, where parameter p is the impedance matrix element with the maximum absolute value. The relative error of 10^{-5} has been used as a stopping criterion for the Bi-CGSTAB. The sparsity of a matrix is defined as the percentage of the number of matrix elements which are above a certain threshold level to the total number of matrix entries. From Tables 1 and 2 we can see that the Coiflet approach has gained a factor of 2 to 5 in CPU time savings over the pulse-based MoM with the LU

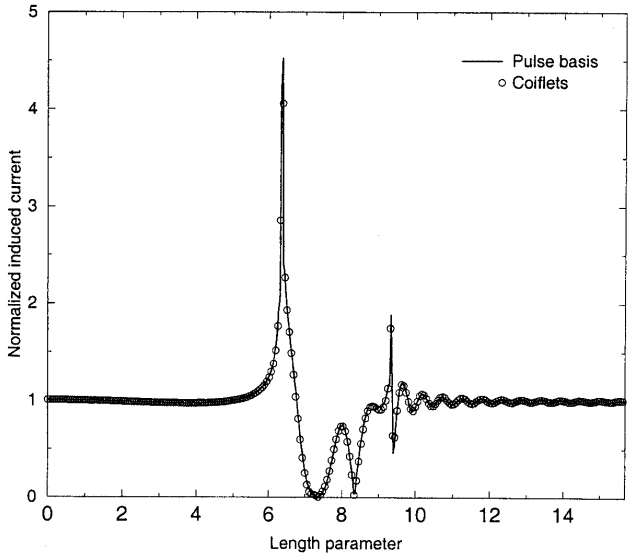

Figure 6. Normalized induced current versus length parameter (λ), TM_z case, $b = 6.34375\lambda$, $h = 1.0\lambda$, $d = 1.0\lambda$, $\phi_{inc} = 60°$, $N_p = 502$, $N_c = 512$.

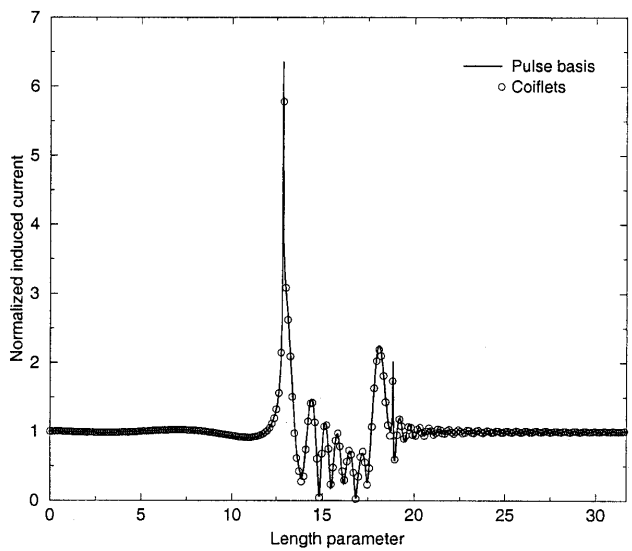

Figure 7. Normalized induced current versus length parameter (λ), TM_z case, $b = 12.84375\lambda$, $h = 2.0\lambda$, $d = 2.0\lambda$, $\phi_{inc} = 60°$, $N_p = 1014$, $N_c = 1024$.

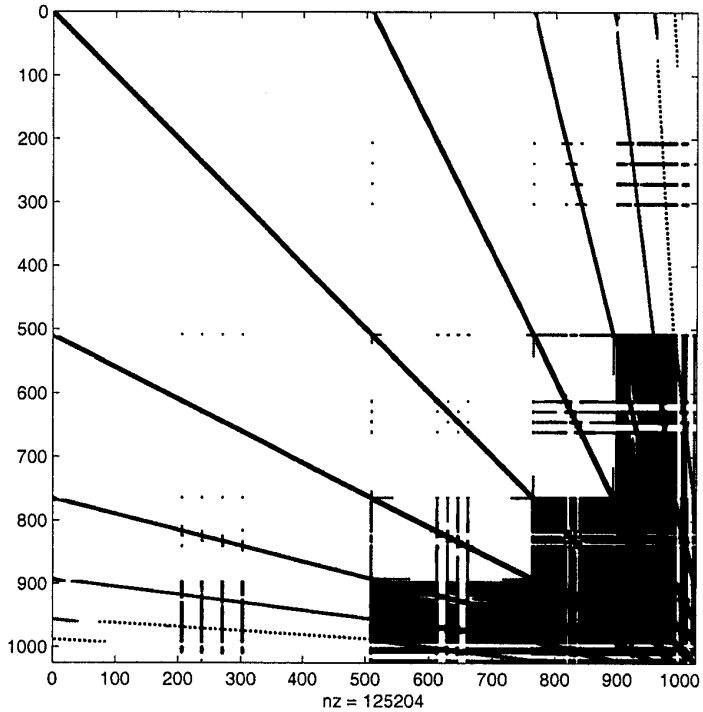

Figure 8. The standard matrix form, TM_z scattering.

decomposition. This achievement is due to the one-point quadrature formula, fast wavelet transform and fast sparse matrix solver.

Figures 6 and 7 show the correction current J_C in the TM_z scattering with the parameters in Tables 1, 2. Figure 8 illustrates the sparse matrix in the standard matrix form with 1024 unknowns and 5 resolution levels.

We also compared results in the far-field zone. We presented here only one example of such comparison. Figure 9 shows the normalized scattering coefficient ($\sqrt{\sigma/\lambda}$), which has been calculated using only the current J_p (13) for the TM_z scattering problem, having the same geometrical parameters as those, used to generate Figure 7.

For all numerical results, presented so far, we implemented the Coiflets with the resolution level $j_0 = 5$. This level has been chosen after a number of numerical tests. It has been noticed that $j_0 = 5$ is the minimum resolution level to achieve a high precision. When we decreased the resolution level to $j_0 = 4$ for the case of Figure 4, we ended with 133 Coifman scaling functions. Correspondingly, we used

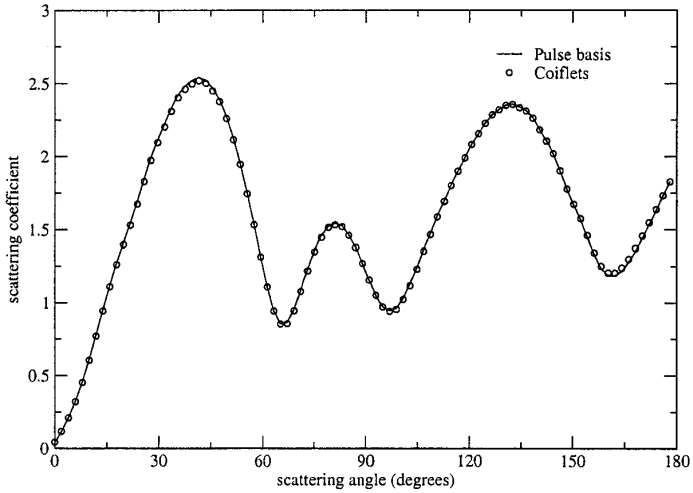

Figure 9. Normalized scattering coefficient $\sqrt{\sigma/\lambda}$ versus scattering angle (in degrees), TM_z case, $b = 12.84375\lambda$, $h = 2.0\lambda$, $d = 2.0\lambda$, $\phi_{inc} = 60°$, $N_p = 1014$, $N_c = 1024$.

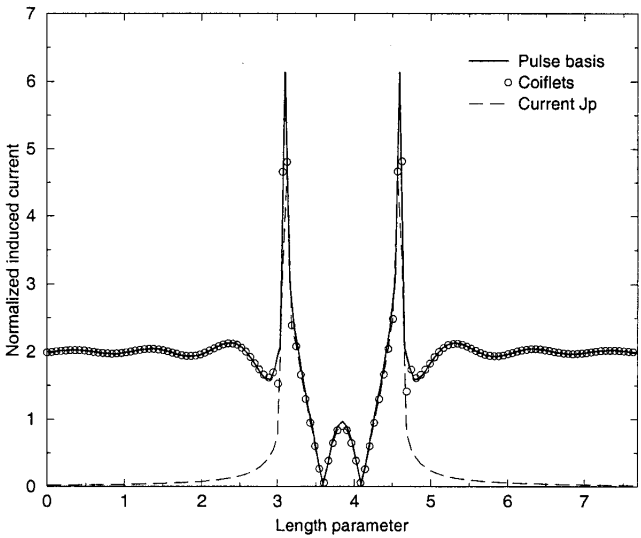

Figure 10. Normalized induced current versus length parameter (λ), TM_z case, $b = 3.09375\lambda$, $h = 0.5\lambda$, $d = 0.5\lambda$, $\phi_{inc} = 0°$, $N_p = 123$, $N_c = 133$.

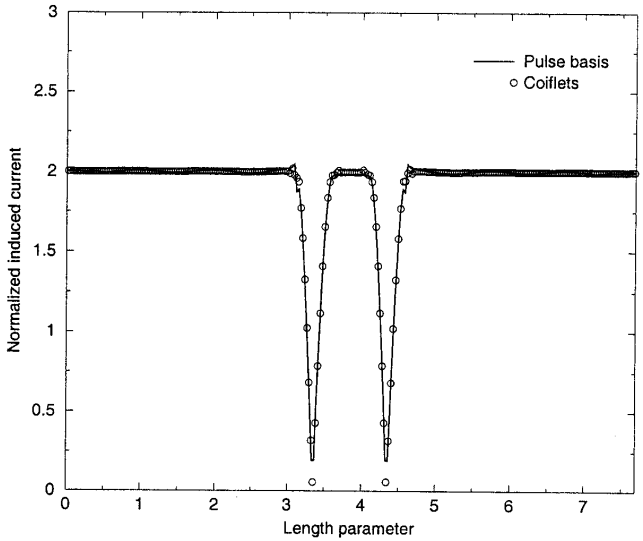

Figure 11. Normalized induced current versus length parameter (λ), TE_z case, $b = 3.09375\lambda$, $h = 0.5\lambda$, $d = 0.5\lambda$, $\phi_{inc} = 0°$, $N_p = 246$, $N_c = 256$.

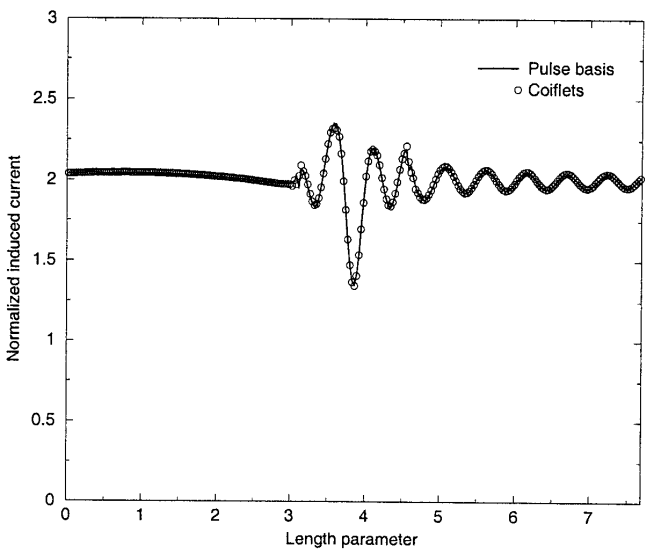

Figure 12. Normalized induced current versus length parameter (λ), TE_z case, $b = 3.09375\lambda$, $h = 0.5\lambda$, $d = 0.5\lambda$, $\phi_{inc} = 60°$, $N_p = 246$, $N_c = 256$.

123 pulse functions to have the results in Figure 10. We still have good agreement between the two approaches, except a small discrepancy at the groove edges. The current J_p is also plotted in Figure 10.

Example 2. TE_z scattering from the groove.

Although, the main emphasis in this paper has been maid on the TM_z case, we also studied the case of TE_z scattering which is not discussed in [1]. Here we present just two numerical results, which are obtained using the following dimensions: $b = 3.09375\lambda$, $h = 0.5\lambda$, $d = 0.5\lambda$. Results are shown in Figures 11 and 12 for two different incident angles.

7. CONCLUSIONS

The Coifman wavelets were employed for the numerical simulation of scattering from a groove in a conducting plane. Under the modified PO-MoM formulation, the compactly supported Coiflets are used on a finite interval without any alteration. The standard Galerkin procedure was used to convert the integral equation into a system of linear algebraic equations. The zero moment property of the Coifman scaling functions leads the single-point quadrature rule for the generation of the majority entries in the MoM matrix. As a result, the new method with double integration is 2–5 times faster then the traditional pulse-δ based MoM of single integration. This superiority over the standard MoM is also due to orthogonality, multi resolution analysis (MRA) and fast wavelet transform of the Coiflets, which generate wavelet sparsified matrix. Additional factor in CPU time savings has been achieved with the use the fast Bi-CGSTAB iterative algorithms.

REFERENCES

1. Shifman, Y. and Y. Leviatan, "Scattering by a groove in a conducting plane: a PO-MoM hybrid formulation and wavelet analysis," *IEEE Trans. Antennas Propagat.*, Vol. 49, 1807–1811, 2001.
2. Harrington, R. F., *Field Computation by Method of Moments*, Macmillan, New York, 1968.
3. Pan, G., M. Toupikov, and B. Gilbert, "On the use of Coifman intervallic wavelets in the method of moments for fast construction of wavelet sparsified matrices," *IEEE Trans. Antennas Propagat.*, Vol. 47, 1189–1999, 1999.

4. Wang, G., "Application of wavelets on the interval to the analysis of thin-wire antennas and scatterers," *IEEE Trans. Antennas Prop.*, Vol. 45, 885–893, 1997.
5. Balanis, C. A., *Advanced Engineering Electromagnetics*, Wiley, New York, 1989.
6. Kantorovich, L. V. and V. I. Krylov, *Approximate Methods of Higher Analysis*, 4th ed., translated by C. D. Benster, John Wiley & Sons, Inc., New York, 1959.
7. Daubechies, I., *Ten Lectures on Wavelets*, SIAM, Philadelphia, 1992.
8. Press, W. H., S. A. Teukolsky, W. T. Vetterling, and B. P. Flannery, *Numerical Recipes in C*, Cambridge University Press, 1992.
9. Van der Vorst, H. A., "Bi-CGSTAB: A fast and smoothly converging variant of Bi-CG for the solution of nonsymmetric linear systems," *SIAM J. Sci. Statist. Comput.*, Vol. 13, 631–644, 1992.
10. Chui, C. K., *An Introduction to Wavelets*, Academic Press, 1991.
11. Chui, C. K., *Wavelets — A Tutorial in Theory and Applications*, Academic Press, 1992.
12. Mallat, S. G., "Multiresolution approximations and wavelet orthonormal bases of $L^2(R)$," *Trans. Amer. Math. Soc.*, Vol. 315, 69–88, 1989.

Youri Tretiakov received the B.Sc. and M.Sc. degrees in electrical engineering, from Moscow Institute of Physics and Technology, Russia, in 1995 and 1997, and the Ph.D. degree in electrical engineering from Arizona State University in 2001. Since 2001 he has been a Staff Engineer with IBM Microelectronics in Burlington, Vermont. His research interests include electromagnetic modeling, CAD tool development for microelectronics, and related areas.

George Pan received the M.S. and Ph.D. degrees in electrical engineering from the University of Kansas, Lawrence, in 1982 and 1984. respectively. From 1984 to 1985, he was a Postdoctoral Fellow at the University of Texas; from 1985 to 1986, he was an Engineer at the Mayo Foundation, Minnesota; from 1986 to 1988, he was an Associate professor at South Dakota State University; and from 1988 to 1995, he was with the University of Wisconsin-Milwaukee, where he was promoted to Professor in 1993. In 1995, he joined Arizona State University, Tempe, as Professor and Director, Electronic Packaging Laboratory of the Electrical Engineering Department.